Deuterons from High-Energy Proton Bombardment of Matter

S. T. BUTLER AND C. A. PEARSON
The Daily Telegraph Theoretical Department, School of Physics, University of Sydney, Sydney, N.S.W., Australia
(Received 13 August 1962)

The results of a process of formation of high-energy deuterons from targets exposed to 25–30 BeV proton beams are evaluated. The formation mechanism involves the pairing of a neutron and proton from the cascade of nucleons which develops within the struck nucleus. The interactions responsible for the deuteron formation are firstly the average nuclear interaction seen by the cascade nucleons within the nucleus, and secondly the normal neutron-proton interaction. A magnitude of 25 MeV for the modulus of the real and imaginary nuclear potentials is sufficient to ensure good agreement with experiment for all energies of the outgoing deuterons and for all emerging angles.

1. INTRODUCTION

IN this paper we amplify our previous remarks[1] concerning the process of formation of high-energy deuterons from targets exposed to 25–30 BeV proton beams.[2,3]

The formation mechanism we propose involves the pairing of a neutron and proton from the cascade of nucleons which develops within the struck nucleus. With this mechanism there is an immediate connection between the momentum distribution of deuterons emerging at a given angle, and the corresponding distribution of protons at that angle. Let the momentum distribution of emerging protons at an angle θ with respect to the incident beam be $p(\mathbf{k})$; it may then be assumed that emerging neutrons have the same distribution.

The interactions responsible for the deuteron formation are firstly the average nuclear interaction seen by the cascade nucleons within the nucleus, and secondly the normal n-p interaction. However, the recoil momentum which the nucleus can absorb in the deuteron formation process is relatively small; similarly the relative momentum of the two nucleons must be small. Hence the deuterons are formed from pairs of neutrons and protons which have roughly equal momenta.

The probability of formation of a deuteron of momentum $\mathbf{K}$ is thus to be expected to be proportional to $p^2(\mathbf{K}/2)$. Other momentum-dependent factors in the proportionality are determined by calculation; the resulting momentum dependence of the deuterons is in good agreement with experiment.

In addition, the deuteron formation probability is proportional to $|V_0|^2$, where $|V_0|$ is the magnitude of the optical potential depth. A quantitative comparison with experimental results thus permits of a determination of $|V_0|$. It is found that in all cases a value of 25 MeV for $|V_0|$ gives excellent agreement between the observed and calculated deuteron momentum distributions. This value of the potential strength is in good agreement with that obtained by Bjorklund *et al.*[4] when fitting the high-energy proton scattering data at 300 MeV. In our case the magnitude $|V_0|$ includes both real and imaginary parts, i.e., it is the magnitude of the full complex potential; the results at 300 MeV indicate[4] that the main contributions must be absorptive and arise from the imaginary term.

The present comparison with experimental results suggests that the main features of the optical potential are energy independent for proton energies between 300 and 900 MeV; the increase in $|V_0|$ over this energy range appears to be at most 10%.

The alternative suggestion that the high-energy deuterons are produced primarily in elementary nucleon-nucleon collisions[5] does not account for the observed features of the deuteron production from nuclei. The ratio of deuterons to protons of the same momentum is found to be approximately constant over a wide energy range.[2] On the other hand, the predictions of the nucleon-nucleon collision model are extremely energy-dependent. Moreover the experimental results include measurements of the momentum spectrum of deuterons emitted at 90° in the laboratory system.[3] Such deuterons cannot come directly from nucleon-nucleon collisions, but must be produced by a secondary process within the nucleus. However, the deuteron and proton momentum spectra are related at 90° in exactly the same way as at the smaller angles and the results at all angles yield an optical potential depth $|V_0| \simeq 25$ MeV.

We, thus, believe that the mechanism considered in this paper, which requires the presence of nuclear matter for the deuteron production, to be the predominant one at all angles.

2. SECOND-ORDER MATRIX ELEMENT—NONRELATIVISTIC

We first perform the nonrelativistic perturbation calculation. The extension to include relativistic effects

[1] S. T. Butler and C. A. Pearson, Phys. Rev. Letters 7, 69 (1961); Physics Letters 1, 77 (1962).
[2] V. T. Cocconi, T. Fazzini, C. Fidecaro, M. Legros, N. H. Lipman, and A. W. Morrison, Phys. Rev. Letters 5, 19 (1960).
[3] V. L. Fitch, P. Piroue, S. T. Meyer, and M. C. Williams (to be published).
[4] F. Bjorklund, I. Blandford, and S. Fernbach, Phys. Rev. 108, 795 (1957).
[5] R. Hagedorn, Phys. Rev. Letters 5, 276 (1960).

can then be carried out quite simply, and we do so in Sec. 4.

Consider two nucleons (neutron and proton) of momenta $\hbar\mathbf{k}_1$ and $\hbar\mathbf{k}_2$, respectively, so that the initial wave function ψ_0 is

$$\psi_0=(1/L^3)\exp[i(\mathbf{k}_1\cdot\mathbf{r}_1+\mathbf{k}_2\cdot\mathbf{r}_2)], \tag{1}$$

where L is the linear dimension of a normalization cube. The final wave function ψ describing a deuteron with momentum $\mathbf{K}$ is then

$$\psi=(1/L^{3/2})\chi(r)\exp(i\mathbf{K}\cdot\mathbf{R}), \tag{2}$$

where $\mathbf{R}$ is the c.m. coordinate $\frac{1}{2}(\mathbf{r}_1+\mathbf{r}_2)$, $\mathbf{r}$ is the relative coordinate $\mathbf{r}_2-\mathbf{r}_1$, and χ is the internal deuteron wave function.

The transition probability $\omega(\mathbf{K})d\mathbf{K}$ that after time t the optical potential $V(r_1)+V(r_2)$, combined with the internal neutron-proton interaction $v(r)$, produces a deuteron of wave vector $\mathbf{K}$ in the interval $d\mathbf{K}$ is

$$\omega(\mathbf{K})d\mathbf{K}=\frac{4|H_{if}^{(2)}|^2}{\hbar^2}\frac{\sin^2(\frac{1}{2}w_{if}t)}{w_{if}^2}\rho(\mathbf{K})d\mathbf{K}. \tag{3}$$

Here $H_{if}^{(2)}$ is the second-order matrix element involving the product (V,v), $\rho(\mathbf{K})$ is the density of final states, and

$$\hbar w_{if}=E_i-E_f,$$

where E_i and E_f are the initial and final energies, respectively.

The second-order matrix element $H_{if}^{(2)}$ is given as

$$H_{if}^{(2)}=\sum_j\frac{H_{ij}^{(1)}H_{jf}^{(1)}}{E_j-E_f}, \tag{4}$$

where $H_{ij}^{(1)}$ and $H_{jf}^{(1)}$ are first-order matrix elements to and from an intermediate state j, respectively. We devote the remainder of this section evaluating $H_{if}^{(2)}$.

There are three types of contributions to (4), corresponding to the three diagrams of Fig. 1. We consider first the term, say $[H_{if}^{(2)}]_1$, for which particle 1, with wave vector $\mathbf{k}_1$, is scattered by $V(r_1)$ into an intermediate state, $\mathbf{k}_1'$, and, thereafter, joined to particle 2 in a deuteron by $v(r)$. For this term we have

$$[H_{ij}^{(1)}]_1=\frac{1}{L^3}\int d\mathbf{r}_1\exp[i(\mathbf{k}_1-\mathbf{k}_1')\cdot\mathbf{r}_1]V(r_1)$$
$$=\frac{1}{L^3}g(|\mathbf{k}_1-\mathbf{k}_1'|), \tag{5}$$

where g is the Fourier transform of V.

Similarly, we have

$$[H_{jf}^{(1)}]_1=\frac{1}{L^3L^{3/2}}\int d\mathbf{r}_1d\mathbf{r}_2\exp[i(\mathbf{k}_1'\cdot\mathbf{r}_1+\mathbf{k}_2\cdot\mathbf{r}_2)]\times v(r)\chi(r)\exp(-i\mathbf{K}\cdot\mathbf{R})$$
$$=\frac{(2\pi)^3}{L^3L^{3/2}}\delta(\mathbf{K}'-\mathbf{K})\int d\mathbf{r}\exp(-i\mathbf{k}'\cdot\mathbf{r})v(r)\chi(r), \tag{6}$$

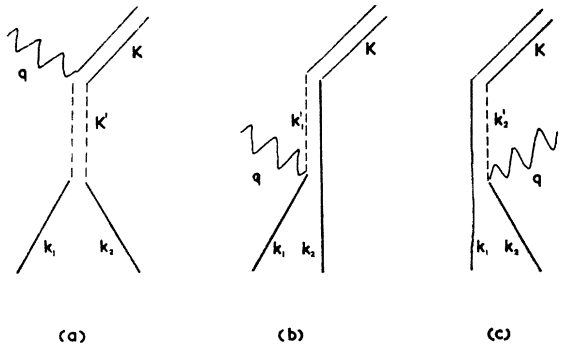

FIG. 1. Diagrams (a), (b), (c) illustrate the simplest means of deuteron formation. $\mathbf{k}_1$, $\mathbf{k}_2$ are the momenta of the proton and neutron in the initial state, $\mathbf{q}$ the recoil of the nucleus, and $\mathbf{K}$ the deuteron momentum in the final state. In case (a) the neutron and proton interact first with each other to form an intermediate deuteron state. This deuteron is then scattered by the nucleus into the final state. In case (b) the neutron is scattered into an intermediate state by an interaction with the nucleus. The scattered neutron and an unscattered proton then interact with each other to form a deuteron. In case (c) a scattered proton pairs with an unscattered neutron.

where

$$\mathbf{K}'=\mathbf{k}_1'+\mathbf{k}_2$$

and

$$\mathbf{k}'=\tfrac{1}{2}(\mathbf{k}_1'-\mathbf{k}_2).$$

If we write $\chi(r)$ in the Hulthèn form

$$\chi(r)=(C/r)(e^{-\gamma r}-e^{-\zeta r}), \tag{7}$$

the integral in (6) can be readily evaluated to be

$$-4\pi C(\hbar^2/m)[1+(k'^2+\gamma^2)/(k'^2+\zeta^2)], \tag{8}$$

where m is the nucleon mass, and $\hbar^2\gamma^2/m$ is the deuteron binding energy. We have actually found the effect of the second term (involving ζ) to be quite small, and hereafter employ simply the asymptotic form for the deuteron wave function. For normalization of χ we have

$$C^2\simeq\gamma^2/2\pi. \tag{9}$$

For the term under consideration, the energy denominator E_j-E_f is simply expressed by noting that $\mathbf{k}_1'=\mathbf{K}-\mathbf{k}_2$. We find

$$E_j-E_f=(\hbar^2/m)[(\tfrac{1}{2}\mathbf{K}-\mathbf{k}_2)^2+\gamma^2]. \tag{10}$$

Thus after summing over intermediate states we find our first contribution $[H_{if}^{(2)}]_1$ as

$$[H_{if}^{(2)}]_1=-\frac{4\pi C}{L^3L^{3/2}}\frac{g(|\mathbf{K}_i-\mathbf{K}|)}{[\mathbf{k}_i+\frac{1}{2}(\mathbf{K}-\mathbf{K}_i)]^2+\gamma^2}, \tag{11}$$

where

$$\mathbf{K}_i=\mathbf{k}_1+\mathbf{k}_2$$

and

$$\mathbf{k}_i=\tfrac{1}{2}(\mathbf{k}_1-\mathbf{k}_2).$$

Thus $\mathbf{K}_i$ and $\mathbf{k}_i$ are the initial c.m. and internal wave vectors of the two free nucleons.

The second contribution, $[H_{if}^{(2)}]_2$, with particle 2 being scattered into the intermediate state $\mathbf{k}_2'$, is

identical to (11) except that $+\frac{1}{2}(\mathbf{K}-\mathbf{K}_i)$ becomes $-\frac{1}{2}(\mathbf{K}-\mathbf{K}_i)$ in the denominator.

Finally the third contribution, in which a virtual deuteron is formed with wave vector $\mathbf{K}'$ in the intermediate state, has matrix elements

$$[H_{ij}^{(1)}]_3=\frac{1}{L^3L^{3/2}}\int d\mathbf{r}d\mathbf{R}\exp[i(\mathbf{K}_i\cdot\mathbf{R}+\mathbf{k}_i\cdot\mathbf{r})]\times v(r)\chi(r)\exp(-i\mathbf{K}'\cdot\mathbf{R})$$
$$=-\frac{4\pi C}{L^3L^{3/2}}\frac{\hbar^2}{m}(2\pi)^3\delta(\mathbf{K}_i-\mathbf{K}')$$

and

$$[H_{jf}^{(1)}]_3=\frac{1}{L^3}\int d\mathbf{r}_1d\mathbf{r}_2\,\chi(r)\exp(i\mathbf{K}'\cdot\mathbf{R})\times[V(r_1)+V(r_2)]\chi(r)e^{-i\mathbf{K}\cdot\mathbf{R}}.$$

We make the approximate replacement $V(r_1)+V(r_2)\simeq 2V(R)$ so that

$$[H_{jf}^{(1)}]_3=(2/L^3)g(|\mathbf{K}_i-\mathbf{K}|).$$

After summing over intermediate states $\mathbf{K}'$ we find

$$[H_{if}^{(2)}]_3=+\frac{2\times 4\pi C}{L^3L^{3/2}}\frac{g(|\mathbf{K}_i-\mathbf{K}|)}{k_i^2+\gamma^2}. \tag{12}$$

The total second-order matrix element is thus

$$H_{if}^{(2)}=\frac{4\pi C}{L^3L^{3/2}}g(2x)\times\left[\frac{2}{k_i^2+\gamma^2}-\frac{1}{(\mathbf{k}_i+\mathbf{x})^2+\gamma^2}-\frac{1}{(\mathbf{k}_i-\mathbf{x})^2+\gamma^2}\right], \tag{13}$$

where

$$\mathbf{x}=\tfrac{1}{2}(\mathbf{K}_i-\mathbf{K}). \tag{14}$$

3. DEUTERON FORMATION PROBABILITY

We now wish to evaluate the probability of deuteron formation when the total number of cascade nucleons of each type per nucleus has the distribution $p(\mathbf{k})d\mathbf{k}$ so that we have $p(\mathbf{k})d\mathbf{k}$ of each type of nucleon with wave vector between $\mathbf{k}$ and $\mathbf{k}+d\mathbf{k}$ within the nucleus at any one time. Thus, we must multiply our transition probability (3) by

$$p(\mathbf{k}_1)d\mathbf{k}_1p(\mathbf{k}_2)d\mathbf{k}_2\left(\frac{L^3}{4\pi R_0^3/3}\right)^2,$$

where R_0 is the nuclear radius, and integrate over all $\mathbf{k}_1$ and $\mathbf{k}_2$.

We wish to find the number of deuterons $n(\mathbf{K})d\mathbf{K}$ which are formed in a time τ for *one* traversal of the nucleus by each pair of nucleons whose c.m. momentum is close to $\mathbf{K}$. Thus we have approximately

$$\tau\simeq 4mR_0/\hbar K, \tag{15}$$

where m is the nucleon mass.

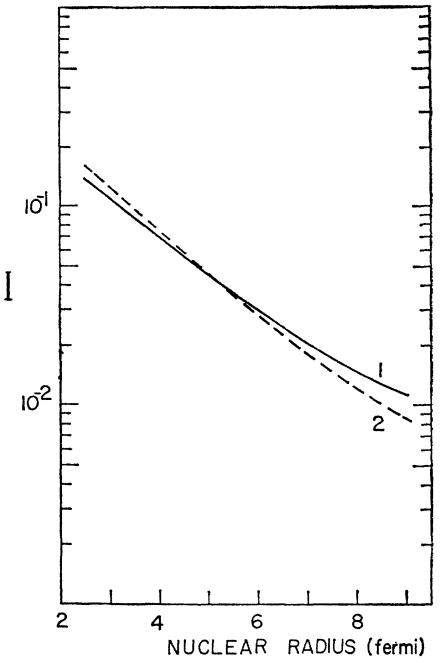

FIG. 2. The function I [Eq. (22)] is plotted as a function of the nuclear radius. The full curve is for a square well, and the dashed for a Saxon potential.

Thus, we finally have a deuteron distribution per nucleus $n(\mathbf{K})d\mathbf{K}$ with

$$n(\mathbf{K})=\left(\frac{L}{2\pi}\right)^3\frac{4}{\hbar^2}\left(\frac{3L^3}{4\pi R_0^3}\right)^2\int d\mathbf{k}_1d\mathbf{k}_2\,p(\mathbf{k}_1)p(\mathbf{k}_2)\times|H_{if}^{(2)}|^2\frac{\sin^2(\frac{1}{2}w_{if}\tau)}{w_{if}^2}, \tag{16}$$

with τ given by Eq. (15).

If we make the transformation $d\mathbf{k}_1d\mathbf{k}_2\rightarrow d\mathbf{K}_id\mathbf{k}_i$, we have $p(\mathbf{k}_1)=p(\frac{1}{2}\mathbf{K}+\mathbf{k}_i+\mathbf{x})$ and $p(\mathbf{k}_2)=p(\frac{1}{2}\mathbf{K}-\mathbf{k}_i+\mathbf{x})$. But in view of the large values of K involved, and the relatively much smaller values of k_i and x, we may clearly take the p factors outside the integral as $[p(\frac{1}{2}\mathbf{K})]^2$.

Thus we find

$$n(\mathbf{K})=(6C/\hbar)^2\frac{1}{(2\pi R_0)^3}[p(\tfrac{1}{2}\mathbf{K})]^2\int d\mathbf{K}_id\mathbf{k}_i[g(2x)]^2\times\left[\frac{2}{k_i^2+\gamma^2}-\frac{1}{(\mathbf{k}_i+\mathbf{x})^2+\gamma^2}-\frac{1}{(\mathbf{k}_i-\mathbf{x})^2+\gamma^2}\right]^2\times\frac{\sin^2(w_{if}\tau)}{w_{if}^2}. \tag{17}$$

We can now integrate immediately over the magnitude of $\mathbf{K}_i$, noting that

$$K_idK_i=(2m/\hbar)dw_{if}. \tag{18}$$

From the energy-conservation factor in (17) we have

$$K_i^2=K^2-4(k_i^2+\gamma^2)\simeq K^2 \tag{19}$$

and thus

$$x=\tfrac{1}{2}|\mathbf{K}-\mathbf{K}_i|\simeq K\sin(\theta/2)\simeq K\theta/2, \tag{20}$$

where θ, the angle between $\mathbf{K}$ and $\mathbf{K}_i$, has very small contributing values.

After performing the integration over w_{if}—which extracts a factor $\frac{1}{2}\pi\tau$—we can also immediately integrate over all angles of $\mathbf{k}_1$, and over the azimuthal angle of $\mathbf{K}_i$. The integration over θ—the angle between $\mathbf{K}_i$ and $\mathbf{K}$—can be taken from $0\rightarrow\infty$, and we find

$$n(\mathbf{K})=2\left(\frac{48\pi Cm}{\hbar^2}\right)^2\left(\frac{V_0}{K}\right)^2 I(R_0)[p(\tfrac{1}{2}\mathbf{K})]^2, \tag{21}$$

where $I(R_0)$ is a dimensionless number, which is, however, a function of R_0. We have

$$I(R_0)=\int_0^\infty \eta d\eta[G(\eta)]^2 \times\int_0^\infty \zeta^2 d\zeta\left[\frac{4}{(\zeta^2+a^2)^2}+\frac{2}{(\zeta^2+\frac{1}{4}\eta^2+a^2)-\zeta^2\eta^2} -\left(\frac{4}{\eta\zeta(\zeta^2+a^2)}-\frac{1}{(\zeta^2+\frac{1}{4}\eta^2+a^2)\eta\zeta}\right)\times\ln\left|\frac{a^2+(\zeta+\eta/2)^2}{a^2+(\zeta-\eta/2)^2}\right|\right]. \tag{22}$$

Here we have defined

$$a=\gamma R_0$$

and

$$G(\eta)=(V_0/4\pi R_0^3)g(\eta/R_0), \tag{23}$$

where V_0 is the central depth of the optical potential. Thus for a square well, for example, we have

$$G(\eta)=(1/\eta^3)(\sin\eta-\eta\cos\eta). \tag{24}$$

The function $I(R_0)$ has been evaluated numerically for a number of different radii using Silliac, both for a square well, and for a Saxon potential with surface thickness 0.6 F. The function is plotted in Fig. 2, and it is seen that the results for the two potential shapes are very similar. The deuteron formation probability is essentially the same in each case, the differences lying within the accuracy of the experimental results with which we shall make comparisons.

All experimental results have been stated in terms of a number of particles per unit solid angle, per unit momentum (1 BeV/c) per circulating proton. Let these distributions be designated n_p and n_d for protons and deuterons, respectively. Then if η be the efficiency of the target, we have

$$n_p(\mathbf{k})=\eta k^2 p(\mathbf{k}),$$

and

$$n_d(\mathbf{K})=\eta K^2 n(\mathbf{K}).$$

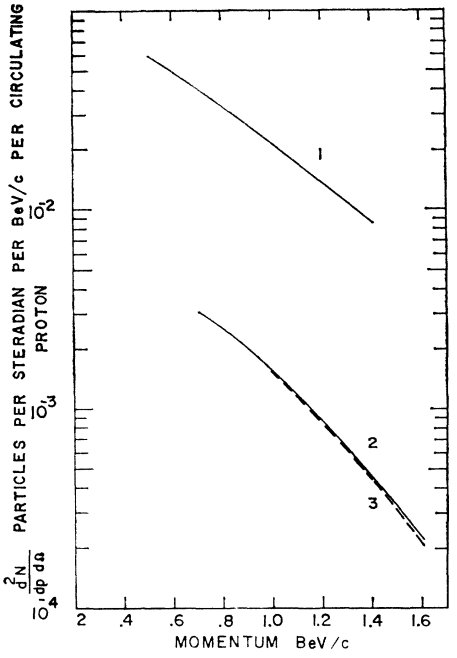

FIG. 3. A comparison of the observed and calculated momentum distributions for deuterons produced from a Be target at an angle of 45° in the laboratory system by protons with incident energy 30 BeV. Curves 2 and 3 are the observed and the calculated deuteron distribution (34). Curve 1 is the experimental distribution of cascade protons used to calculate (34). The experimental data are those of Fitch *et al.* (reference 3).

If we also multiply the deuteron numbers by the spin factor $\frac{3}{4}$, we have finally

$$n_d(\mathbf{K})=\frac{3\pi(48)^2}{\eta}\left(\frac{\kappa}{K}\right)^4\left(\frac{\gamma}{\Lambda}\right)I(R_0)[n_p(\tfrac{1}{2}\mathbf{K})]^2, \tag{25}$$

where $\kappa^2=mV_0/\hbar^2$ and where Λ is a wave number corresponding to 1 BeV/c. The value of the efficiency for the Brookhaven experiments[3] is thought to be approximately $\frac{1}{2}$, i.e., $\eta\simeq\frac{1}{2}$.

4. RELATIVISTIC CORRECTIONS

A relativistic calculation is simplified enormously by the fact that contributions to our matrix elements arise only from small relative momenta (internal deuteron momenta). Thus it is only the c.m. motion of the two nucleons which must be treated relativistically. Only one time t need be considered, which we still measure in the laboratory system—i.e., in the frame of reference in which the optical potential is at rest. All relativistic corrections then appear in terms of the factor Γ, with

$$\Gamma=(1-V^2/c^2)^{-1/2}\simeq(1-v_1^2/c^2)^{-1/2}\simeq(1-v_2^2/c^2)^{-1/2}, \tag{26}$$

where V is the c.m. velocity of the two nucleons (almost unchanged by the deuteron formation), and v_1 and v_2 are the initial velocities of the two nucleons, respectively.

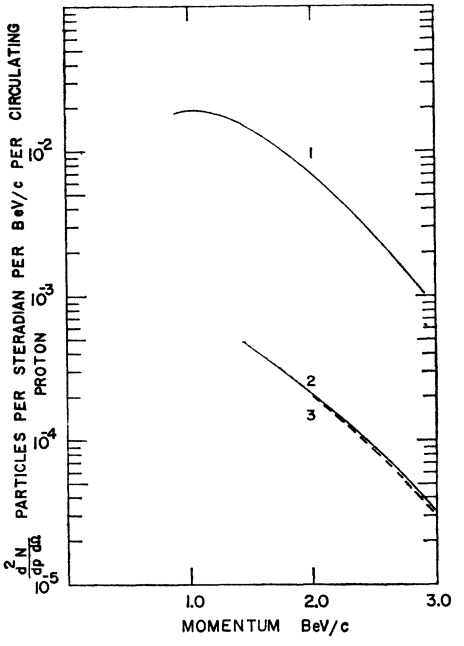

FIG. 4. As in Fig. 3, the deuterons are produced from a Be target at an angle of 30° in the laboratory system by protons with incident energy 30 BeV. The curves are labeled as in Fig. 3, and the experimental results are those of Schwarzschild and Zupančič (reference 6).

There are several points in the calculation at which Γ factors arise:

(1) Energy Denominators

Consider, for example, the energy denominator (10) relating to the matrix element $[H_{if}^{(2)}]_1$. This has the relativistic form

$$E_j-E_f=(\hbar^2k_1'^2c^2+m^2c^4)^{1/2}+(\hbar^2k_2^2c^2+m^2c^4)^{1/2}-(\hbar^2K^2c^2+M^{*2}c^4)^{1/2}, \quad (27)$$

where M^* is the deuteron mass, and m the nucleon mass.

We recall that $\mathbf{k}_1'=\mathbf{K}-\mathbf{k}_2$. We know that contributions arise from $\mathbf{k}_2\simeq\frac{1}{2}\mathbf{K}$, and can, therefore, expand the terms of (27) around $\mathbf{k}_2=\frac{1}{2}\mathbf{K}$, and also in terms of the binding energy ϵ of the deuteron. We find

$$E_j-E_f=c^2[\hbar^2(\tfrac{1}{2}K)^2c^2+m^2c^4]^{-1/2}\times[\hbar^2(\tfrac{1}{2}\mathbf{K}-\mathbf{k}_2)^2+m\epsilon]$$
$$=(1/\Gamma)(\hbar^2/m)[(\tfrac{1}{2}\mathbf{K}-\mathbf{k}_2)^2+\gamma^2]. \quad (28)$$

This is the same as the nonrelativistic result (10), apart from the factor $1/\Gamma$. The same is true for the other energy denominators.

(2) Internal Deuteron Coordinates

The deuteron wave function χ now assumes its simple spherically symmetrical form only in terms of the relative coordinate, say $\mathbf{r}'$, in the frame of reference in which the center of mass is at rest. Thus

$$\chi(\mathbf{r})=Ce^{-\gamma r'}/r'$$
$$=\frac{C\exp\{-\gamma[x^2+y^2+\Gamma^2z^2]^{1/2}\}}{\{x^2+y^2+\Gamma^2z^2\}^{1/2}},$$

where (x,y,z) are the Cartesian components of $\mathbf{r}$, and z is the direction of motion of the center of mass. The requirement that χ be normalized to unity in the laboratory system thus yields

$$C^2\simeq 2\pi\Gamma/\gamma \quad (30)$$

in place of (9).

(3) Matrix Elements

Each matrix element of the form

$$M=\int d\mathbf{r}\exp(i\boldsymbol{\lambda}\cdot\mathbf{r})v(\mathbf{r})\chi(\mathbf{r})$$

now has $v(\mathbf{r})$ and $\chi(\mathbf{r})$ simply expressed in terms of $\mathbf{r}'$. By changing the variable of integration form $\mathbf{r}$ to $\mathbf{r}'$ we have

$$M=\frac{1}{\Gamma}\int d\mathbf{r}'\exp(i\boldsymbol{\lambda}'\cdot\mathbf{r}')v(\mathbf{r}')\chi(\mathbf{r}'),$$

where $\boldsymbol{\lambda}'$ is related to $\boldsymbol{\lambda}$ by Lorentz transformation. Thus by the evaluation as carried out previously, we have

$$M=-(1/\Gamma)4\pi C\hbar^2/m, \quad (31)$$

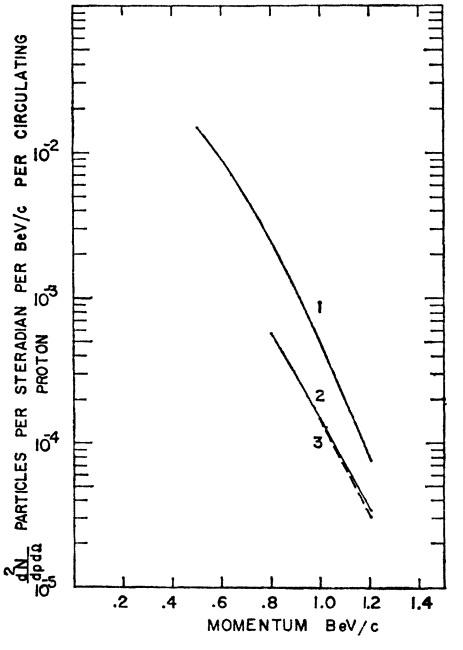

FIG. 5. As in Fig. 3, the deuterons are produced from a Be target at an angle of 90° in the laboratory system by protons with incident energy 30 BeV. The curves are labeled as in Fig. 3, and the experimental data are those of Fitch *et al.* (reference 3).

which replaces (8). This factor of $1/\Gamma$ is cancelled by that from the energy denominators.

(4) Integration over K_i

Instead of (18) we now find

$$K_i dK_i = (2m/\hbar)\Gamma dw_{if}. \tag{32}$$

(5) Time τ of Nuclear Traversal

Instead of (15) we now have

$$\tau \simeq 2R_0/V = 4mR_0\Gamma/\hbar K. \tag{33}$$

After collection of all Γ factors, we find that the deuteron formation probability is multiplied by Γ^3. Thus our final result is

$$n_d(\mathbf{K}) = \frac{3\pi}{\eta}(48)^2\left(\frac{\kappa}{K}\right)^4\left(\frac{\gamma}{\Lambda}\right)\left(\frac{\hbar^2K^2}{4m^2c^2}+1\right)^{3/2} \times I(R_0)[n_p(\tfrac{1}{2}\mathbf{K})]^2. \tag{34}$$

5. RESULTS

By choosing as the radius for the target nucleus $R_0 = 1.2A^{1/3}$ F and using the appropriate value for $I(R_0)$ from Fig. 2, we have compared the expression for the expected deuteron momentum spectrum (34) with those measured at various angles. These comparisons are shown in Figs. 3–8, together with the experimental proton distributions which have been substituted in (34).

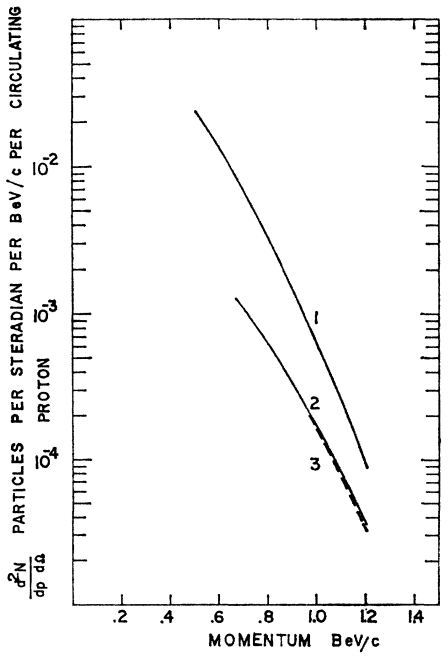

FIG. 6. A comparison of the observed and calculated momentum distributions for deuterons produced from an Al target by protons with incident energy 30 BeV at an angle of 45° in the laboratory system. The curves are labeled as in Fig. 3. The experimental results are those of Fitch *et al.* (reference 3).

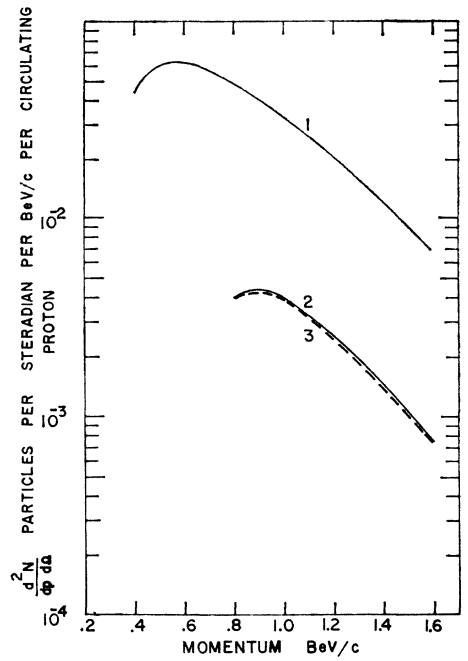

FIG. 7. As in Fig. 3, the deuterons are produced from a Be target at an angle of 90° in the laboratory system by protons with an incident energy of 10 BeV. The curves are labeled as in Fig. 3, and the experimental results are those of Fitch *et al.* (reference 3).

By comparing (34) with the observed deuteron momentum distributions we can determine the magnitude and energy dependence of the optical potential strength $|V_0|$ which are necessary to fit the experimental results. In Figs. 3–6 we have used for the magnitude of the optical potential at all energies the constant value $|V_0| = 25 \pm 5$ MeV found by fitting the expression (34) to the observed number of deuterons with momentum 1.1 BeV/c scattered from a Be target at an angle of 45° in the laboratory system shown in Fig. 3. The target efficiency was taken to be 50%.

In Figs. 3, 4, and 5 the expression (34) is compared with the experimental deuteron distributions from a Be target struck by 30-BeV primary protons, observed at angles of 45°, 30°, and 90° in the laboratory system. The experimental results in Figs. 3, 5, 6, and 7 are those of Fitch *et al.*[3] and in Fig. 4 those of Schwarzschild and Zupančič.[6] In Fig. 6 the expression (34) is compared with the experimental results for deuterons produced (at an angle of 45° in the laboratory system) from an Al target by protons with incident energy 30 BeV; the same value of $|V_0|$ is employed.

In Fig. 7 the expression (34) is compared with the number of deuterons produced from a Be target at 90° by protons with incident energy 10 BeV. Since the efficiency of the target was not known for 10-BeV

[6] A. Schwarzschild and Č. Zupančič (to be published).

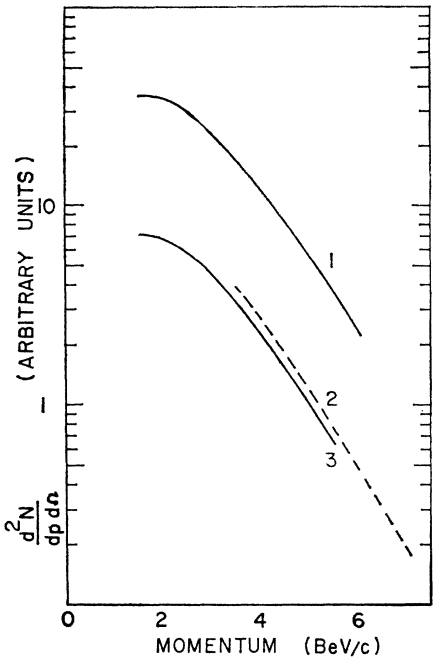

FIG. 8. A comparison of the calculated deuteron momentum distribution (34) with that observed for deuterons produced from Al and Pt targets at an angle of 16.9° in the laboratory system by Cocconi *et al.* (reference 1). Curve 1 is the experimental distribution of cascade protons used to calculate (34). Curves 2 and 3 are the calculated expression (34) and the observed deuteron momentum distribution. Because the experimental proton distribution employed was unnormalized, all the curves are in arbitrary units.

protons the calculated and experimental curves were made to correspond at 1 BeV/c.

In Fig. 8 the expression (34) is compared with the deuteron distribution measured at CERN by Cocconi *et al.* Here the deuterons were observed at an angle of 10.9° and the energy of the incident protons was 25 BeV. Because the measured proton distribution was not normalized in this experiment all the curves are plotted in arbitrary units.

In all the cases shown in Figs. 3 to 8 the expression (34) satisfactorily represents the measured deuteron momentum distribution, if $|V_0|$ is taken to be a constant independent of energy. At 90° deuteron production from direct nucleon-nucleon collisions is kinematically forbidden, and deuterons must necessarily be produced by a secondary process such as we have described. The expression (34) reproduces not only the momentum spectrum of deuterons at 90° in the laboratory system, but also reproduces the spectra of those deuterons observed at smaller angles using the same value of $|V_0|$. It seems clear that the mechanism we have described must be responsible for the majority of deuterons at all angles.

The value of $|V_0|$, 25±5 MeV, used to fit the experimental data in Figs. 3–6 is the same as that found from a previous analysis of the emulsion data and is in reasonable agreement with the (mainly absorptive) potential used by Bjorklund *et al.* to fit the proton scattering data at about 300 MeV.

The result (34) depends on the radius of the target nucleus through the integral I and through the flux of cascade protons $n_p(\frac{1}{2}\mathbf{K})$. Cocconi *et al.*[2] found that the ratio of deuterons to protons of the same momentum increased slightly with increase in the radius of the target nucleus. The value of I decreases rather rapidly with this radius, and we are, therefore, dependent on the observed $n_p(\frac{1}{2}\mathbf{K})$ increasing sufficiently with nuclear radius to be consistent with the CERN result.

It must be remembered, however, that in our model we have obtained the incident flux by assuming that the protons in the nucleon cascade are scattered randomly throughout the nuclear volume. It would probably be more realistic to imagine that the nucleon cascade occupies only part of the nuclear volume and that as the target nucleus increases in size, the volume occupied by the nucleon cascade increases more slowly than the nuclear volume. The flux of incident neutrons and protons representing the nucleon cascade in the model would be consequently increased and the enhanced deuteron production could also contribute to the CERN result.

Such an improvement in the model could perhaps effect a small reduction in the depth $|V_0|$ of the optical potential we have used to fit the expression (34) to the experimental results, although such an alteration would not affect the energy dependence of this potential.

The magnitude of the optical potential necessary to explain the observed deuteron momentum spectra is approximately constant for incident nucleon energies between 300 and 3000 MeV.

The authors are indebted to Professor H. Messel for his enthusiastic support. This work was supported in part by the Nuclear Research Foundation within the University of Sydney.